A Combined High-Resolution X-ray Powder Diffraction, Computational, and XPS Study of the Local Structure of Extra-Framework Copper Ions in Over-Exchanged Cu-MCM22 Zeolite

Marco Milanesio,*,† Gianluca Croce,† Davide Viterbo,† Heloise O. Pastore,*,‡ Artur J. dos Santos Mascarenhas,‡ Erica C. de Oliveira Munsignatti,‡ and Laura Meda§

Dipartimento di Scienze e Tecnologie Avanzate and Nano-SiSTeMI Interdisciplinary Centre, Università del Piemonte Orientale "A. Avogadro", Via Bellini 25/G, 15100 Alessandria, Italy, Instituto de Química, Universidade Estadual de Campinas, CP 6154, CEP 13084−971, Campinas, SP, Brazil, and Nano-SiSTeMI Interdisciplinary Centre and Instituto ENI Donegani via Fauser 4, 28066 Novara, Italy

Received: April 25, 2008

Local structure and site distribution of extra-framework copper ions in over-exchanged Cu-MCM22 zeolite were determined by a combination of high resolution X-ray powder diffraction and computational analysis. X-ray diffraction data suggested the presence of three Cu sites in six-membered rings and one site in a five-membered ring close to the interlamellar region, inside the MCM-22 supercage, whereas no Cu ions were found within the sinusoidal channels. First principle molecular orbital DFT calculations were employed to obtain, for the first time, an accurate structural description of the Cu(I) sites in the supercage, adding a structural and energetic interpretation to previous IR and EPR studies. The combined experimental and computational study suggested that Cu(I) sites facing 6-MRs are particularly stable. In general 5- or 4-fold coordination sites are located in 6-MRs while 2- or 3-fold coordination sites are located in 5-MRs. Three preferentially occupied sites were found in copper-exchanged MCM-22. X-ray photoelectron spectroscopy suggested the formation of dispersed Cu close to the surface of MCM-22 crystallites, easily reduced to Cu(I) under ultrahigh vacuum conditions.

1. Introduction

MCM-22 zeolite (IZA code MWW) was discovered in 1990 by Mobil researchers. The as-prepared material, or precursor, is an HMI-containing (HMI = hexamethyleneimine) layered solid that transforms into a zeolitic structure upon calcination. The layers display sinusoidal channels with 10-membered rings (MRs).[2−4] The surface of the layers shows external pockets that form large cavities when the layers condense into the final three-dimensional structure.[3] The calcined MCM-22 presents two nonintersecting pore systems, both accessible through 10-MRs.[5,6] One of them is made of a two-dimensional system of sinusoidal channels and the other channel system consists of large supercages delimited by 12-MRs in the widest part. This particular combination of large- and medium-pore channels in the calcined material was previously proposed on the basis of the results of model reactions[7] and then confirmed by X-ray powder diffraction analysis from synchrotron radiation and high resolution TEM data.[5]

Cu-exchanged MCM-22 proved to be a very interesting catalyst in NO_x decomposition, even in the presence of water in the reactant stream,[8,9] a reaction of utmost relevance for the abatement of these pollutants. MCM-22 has also been used in an important industrial process such as benzene alkylation with propene to produce cumene.[10] One application is known for Cu-MCM-22 as additive to fluid cracking catalysts.[11] Information on the adsorption properties and reactivity of Cu-exchanged MCM-22 were obtained by FTIR studies of adsorbed CO and NO,[12] which indicated the presence of at least two isolated Cu(II) sites, the precise coordination number and geometry of which could not be determined by infrared spectroscopy alone. Upon reduction of Cu(II) in vacuum, the NO adsorption showed two distinct Cu(I) sites, which converted rapidly into Cu(II) sites in the presence of NO at room temperature. Infrared spectra of CO adsorbed on these samples showed, besides isolated copper sites, an absorption assigned to cationic Cu-clusters present only in over-exchanged samples, which resulted in the more active catalysts.[13]

Several cation sites have been proposed in the literature for metal-exchanged MCM-22 by the use of different investigation techniques. Wasowicz et al.[14] proposed three different cation sites (S_I, S_{II}, S_{III} in the supercage shown in Figure 1) for Cu(I) in MCM-22 through an electron spin resonance (ESR) and electron spin echo modulation (ESEM) spectroscopy study. The same authors[15] proposed one additional site (S_V in Figure 1) and explored the possible variations of the four sites in the supercage, plus one (S_{IV}, not shown) in the sinusoidal channel (see Figure 10 in ref 15). A more recent paper[16] reported on the EPR investigation of Cu(I)−NO complexes in MCM-22, and suggested two generic possible Cu locations, one close to S_{II} and the second close to S_I (see Figure 2 in ref 16). Besides these suggestions, no quantitative geometry and energetic data are available on the local environment of copper in MCM-22. The present paper provides for the first time this geometry and energetic information for all the Cu insertion sites in the supecage, as the result of complementing the diffraction analysis with exhaustive density functional theory (DFT) calculations carried out on extended cluster models.

* To whom correspondence should be addressed. E-mail: marco.milanesio@mfn.unipmn.it (M.M.) and gpmmm@iqm.unicamp.br (H.O.P.).
† Università del Piemonte Orientale "A. Avogadro".
‡ Universidade Estadual de Campinas.
§ Instituto ENI Donegani.

10.1021/jp803619r CCC: $40.75
Published on Web 08/19/2008

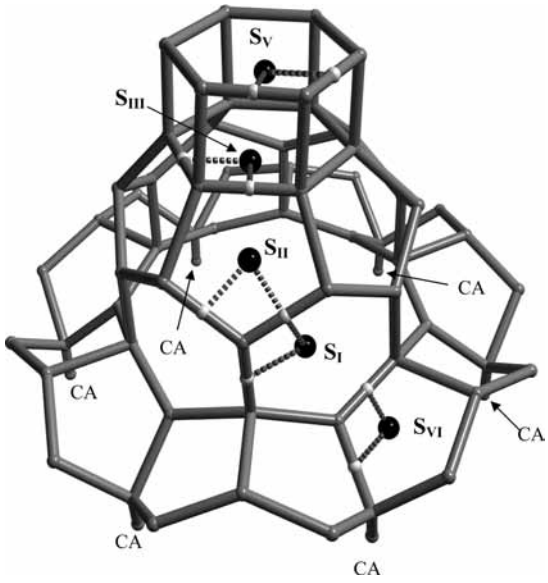

Figure 1. Location and labeling of copper sites within the supercage; only one half of the supercage is depicted, the second half is obtained by mirror symmetry (oxygen atoms omitted for the sake of clarity).

Figure 1 shows the supercage in which the proposed sites S_I, S_{II}, S_{III}, S_V, and S_{VI} (considered for the first time in the present paper) are located while S_{IV} is in the sinusoidal channel. All the sites in the supercage can be grouped into two families: Cu ions in sites S_I, S_{III}, and S_V are coordinated to six-membered rings (6-MR), while Cu ions in sites S_{II} and S_{VI} are stabilized by the five-membered rings (5-MR) of the framework. Finally, it is worth recalling the results of a ^{129}Xe NMR study suggesting that, at low Xe pressure, gas adsorption was observed only in the large cages of MCM-22,[17] where a stronger acidity was found.[18] Theoretical investigations,[18,19] have been carried out, also in combination with NMR,[20] to shed light on the metal distribution and acidity strength of B, Al, Ga, and Fe, inserted in the MCM-22 framework. To our knowledge, extra-framework Cu sites inside the MCM-22 supercage were never studied by computational techniques. Conversely, Cu sites in other zeolites, different from MCM-22, were widely investigated in the last decade, and differently coordinated Cu(I) sites were found for CHA,[21] MFI,[22,23] and FER,[23,24] zeolites with medium-high Si/Al ratio, by using both experimental (i.e. luminescence or infrared spectroscopy) and theoretical approaches. Finally, to obtain information on the geometry features of these sites, X-ray absorption spectroscopy has also been used.[25,26] To our knowledge, structural investigations of Cu sites in zeolites using X-ray[27] and neutron[28,29] diffraction techniques, have been carried out only on Cu−Y zeolite, where the lower Si/Al ratio allowed the insertion of larger amounts of copper. Cu−Y zeolite was also studied by computational techniques.[30]

Concerning the amount of copper in Cu-exchanged (in $Cu(NO_3)_2$ solution) MCM-22 samples with Si/Al ratio equal to 15, three situations could be envisaged, since, in principle, each Cu(II) must be neutralized: (i) at Cu/Al molar ratios smaller than 0.5, isolated Cu ions would be most probable; (ii) at Cu/Al molar ratios slightly larger than 0.5, monocationic dimers[31] are probably found; (iii) at high Cu excess, separate dense Cu phases (CuO) would form. Previous studies by some of us[13] showed that the sample pretreatments, under either argon or oxygen, led to different reactivity of Cu species towards NO. The maximum amount of copper [nominally Cu(II)/Al ratio equal to 0.5] that could be introduced into the MCM-22 channels, without formation of a separated copper oxide phase, was deduced by analyzing a series of under- and over-exchanged Cu-MCM22 samples by X-ray diffraction and resulted in a Cu(II)/Al ratio equal to 0.71.[32]

In the present work, over-exchanged samples (Cu/Al ratio equal to 0.71, see section 2.1 for details) have been studied by high resolution X-ray powder diffraction (HR-XRPD) after both complete oxidation and reduction of copper, along with ab initio calculations, in order to explain the copper distribution in Cu-MCM22 zeolites. In fact molecular orbital calculations allowed a careful geometry and energetic characterizations of the Cu(I) environment in the MCM-22 channels. Finally, X-ray photoelectron spectroscopy (XPS) has been employed to understand the distribution and chemical state of copper present at the surface of the MCM-22 crystallites.

2. Experimental Section

2.1. Sample Synthesis. Zeolite MCM-22 was prepared by hydrothermal treatment of a gel with the following composition: 4.44 Na_2O:30 SiO_2:Al_2O_3:17.76 HMI:889 H_2O, at 423 K and stirring at 60 rpm for 7 days. The obtained material was thoroughly washed, dried, and calcined at 853 K under dry oxygen to obtain the acid form of MCM-22 (named H-MCM22). The calcined sample was first exchanged with a solution of $NaNO_3$ 0.1 mol L^{-1} and subsequently exchanged with a solution 0.01 M of $Cu(NO_3)_2 \cdot 3H_2O$, for 24 h at room temperature. The under-exchanged Ox-CuMCM22-50 sample, employed in the XPS analysis only, was prepared by using stoichiometric amounts of Cu needed to occupy half of the available sites. Then, in a second series of samples, the amount of copper solution was adjusted to obtain a nominal Cu/Al atomic ratio equal to 0.75. Since each doubly positive Cu(II) ion counterbalances two AlO_4^- sites, such ratio results in an over-exchanged sample with a percentage of Al sites balanced by Cu(II) cations equal to 150% in terms of charge. To obtain over-exchanged samples, the pH was adjusted to 7.5 with a NH_4OH solution as reported in ref 31. The elemental analysis showed that a ratio of 0.71 was finally obtained (142% exchanged sample), which led to a sample with the largest copper concentration without separation of dense CuO phases. The unit cell formula was $Cu_{2.27}[Al_{4.54}Si_{67.46}O_{144} \cdot 0.46CuO]$.

This Cu-exchanged MCM-22 sample was washed, dried, and calcined at 773 K under oxygen for 6 h. Then two sets of quartz capillaries (diameter 1 mm) were filled with the Cu-exchanged MCM-22 samples. The first set was connected to a vacuum line and heated at 823 K for 5 h in 100 torr of oxygen (and changing at least twice the oxygen), and cooled down to room temperature under oxygen before the final outgassing. This procedure allowed us to obtain the oxidized (from now on referred as "Ox-CuMCM22") Cu-MCM22 sample. The second set was heated at 823 K for 5 h in vacuum to obtain the reduced Cu-MCM22 sample ("Red-CuMCM22"). After the treatments, the capillaries were sealed to prevent contamination due to air moisture. This procedure assured that all electron density found in the channels after Rietveld refinement could be assigned to copper ions.

2.2. Data Collection and Refinement. High-resolution X-ray powder diffraction (HR-XRPD) data were collected by the Swiss−Norwegian beamline BM1b[33] of the European Synchrotron Radiation Facility (ESRF, Grenoble) on the Ox-CuMCM22 and Red-CuMCM22 samples in order to locate the Cu cation sites. The parent H-MCM-22, that is, the sample before Cu-exchange, was used as reference material. The *P6/mmm* structure of the calcined MCM-22 exposed to air, determined by Leonowicz et al.[5] was used as the starting model (considering framework Si and O atoms only), and the Rietveld refinement

TABLE 1: Agreement Factors (*R*wpb as Defined in GSAS Manual[34]), Lattice Parameters (Å) and Occupied Extra-Framework Sites Suggested by the Rietveld Refinement, with the Indication of the Relative Peak Height[a]

		lattice parameters		height of Cu sites in difference Fourier
sample name	*R*wpb	*a* (Å)	*c* (Å)	
H-MCM22 in vacuum	0.106	14.193(1)	25.039(8)	
Ox-CuMCM22-50	0.103	14.190(1)	25.014(2)	S_{III}, S_V
Ox-CuMCM22	0.098	14.182(1)	25.049(8)	S_{III}, $S_V > S_I$, S_{II}
Red-CuMCM22	0.098	14.187(1)	25.070(8)	S_{III}, $S_V > S_I$, S_{II}

[a] Site labeling as given in Figure 1.

of all the structures was carried out using the GSAS software.[34] The profile function number 4 (as defined in the GSAS software) was employed because it allowed anisotropic broadening refinement (mandatory because of the lamellar features of the samples), thanks to its definition as a convolution between a pair of back-to-back exponentials and a pseudo-Voigt.[34] The cell parameters, the positions, and ADP parameters of the Si and O atoms were refined, restraining the Si−O and the O−O distances to the average values of 1.60 and 2.61 Å, respectively, and constraining the ADP parameters of each atom species to a single value, which converged to 0.034(5) and 0.031(6) Å^2 for Si and O, respectively. The location of the copper ions was then obtained by difference Fourier syntheses, on the basis of the extra-framework electron density peaks interpreted as copper sites (see Table 1). The parameters of the Cu atoms were kept constant (ADP equal to 0.12 and occupancy equal to 0.04 to account for the disorder as described in section 3.1) in the final refinement. Their insertion resulted in better agreement values, but attempts at refining their positions and occupancy at the same time resulted in an unstable refinement with large estimated standard deviation values, because of the small amount of copper and its disorder (see section 3.1 for more details on copper locations). Therefore the positions were kept fixed to those indicated by the DFT calculations and only the occupancy was refined (see Table 2).

2.3. Computational Details. Molecular orbital calculations were performed with the Jaguar software[35] employing the DFT method based on Becke's exchange[36] and the Lee, Yang, Parr correlation functional[37] (BLYP). The Cu, Si, and Al atoms were described using the LAV3P relativistic effective core potential (ECP).[38] The other atoms were described using the 6-31G (method labeled LAV3P in Table 3 and its discussion) and 6-31G(d) (method named LAV3P* in Table 3 and its discussion) basis sets.[39] The BLYP functional and the LAV3P* ECP were chosen because they gave reliable results in the study of copper insertion in zeolites different from MCM-22, with a limited computation time demand.[21,40] The dangling bonds resulting in the cluster model after extraction from the periodic crystal structure of MCM-22, were saturated with H atoms. The positions of the six H atoms (labelled CA in Figure 1) substituting the oxygen atoms sitting on the mirror plane and connecting the two halves of the supercage belonging to different MCM-22 layers, were fixed during the first geometry optimizations (aimed at locating the stable Cu sites) to fully maintain the original overall shape of the MCM-22 supercage. Then the constraints were removed in the final geometry optimizations (aimed at characterizing the geometry and energetic features of the Cu sites), and a full geometry optimization was carried out. No significant distortions with respect to the supercage shape in the periodic MCM-22 crystal structure were observed. Graphical manipulations and molecular pictures were carried out using the softwares MOLDRAW[41] and MAESTRO.[42]

2.4. XPS Analysis. The XPS analysis was carried out by a monochromatized PHI-5500 instrument with Al source. The analyses were performed at 300 Watt, with a pass energy of 58.7 eV, at a take-off angle of 45°. The vacuum in the chamber was maintained around 10^{-9} Torr during the measurement. Powder samples were pressed on Indium supports to have a flat surface. An electron gun was used to compensate the surface positive charge during the measurements. The area of the samples was relatively large (0.5 mm^2) and the estimated sampling depth was around 5 nm. Assignment of atomic species on the basis of their chemical shift has been made by standard reference data.[43]

3. Results and Discussion

3.1. Rietveld Refinement and Copper Location. At first, a calcined H-MCM22 sample was sealed in a capillary after further outgassing at 423 K for 5 h, and its diffraction pattern was compared to that of a calcined sample exposed to air, in order to optimize the refinement strategy and to check if the sample preparation was successful. In the calcined sample exposed to air the residual electron density map (obtained by difference Fourier syntheses) showed many peaks due to extra-framework matter, mainly constituted by water molecules. The calculated and observed diffraction patterns for the calcined, vacuum-sealed H-MCM22 sample were in good agreement indicating that (i) no residual electron density (except for a very small spurious peak located at the center of the supercage present in all the samples, irrespective of the Cu content and of the exposition or not to air moisture) was present in the MCM-22 channels and (ii) the sample preparation was effective in eliminating organic residues and adsorbed water molecules. Conversely, after full profile refinement of the XRPD patterns collected on the vacuum-sealed Cu-exchanged MCM-22 samples, difference Fourier syntheses allowed to locate significant extra-framework electron density peaks, which were interpreted as copper sites. These peaks were not observed in the calcined, vacuum-sealed H-MCM-22 and are different from the peaks found in the sample exposed to air, which were assigned to water molecules.[5]

The coordinates of the five Cu insertion sites are given in Table 2. The insertion in the Rietveld refinement of the Cu atoms with fixed positions, ADP (0.12 because of the disorder) and occupancy [0.04, resulting from the ratio of the number of Cu atoms in the cell (2.27) and the total multiplicity of the Cu sites imposed by symmetry (Table 2)] resulted in a small improvement of the agreement factors. Any attempt at refining both their positions and their occupancy gave unstable results, probably because of the small amount of copper and of the fact that, as often observed,[44] the extra-framework species do not obey the high *P6/mmm* symmetry, which is mandatory for a stable refinement. However the qualitative evidence that the occupancy of sites S_{III}, $S_V > S_I$, S_{II} could be accounted for by the fact that S_{III} and S_V appear in all data sets irrespective of the Cu content and their height in the Fourier synthesis resulted larger. The relative heights, observed for the different sites, can also be ascribed to the average distance of the different Cu positions, as precisely located by the DFT calculations (vide infra), from the 6-fold axis. Indeed, sites S_{III} and S_V are close (∼0.45 Å) to the 6-fold axis (site symmetry *6mm* with multiplicity 2) and the center of mass of the six overlapping electron density peaks resulted on the 6-fold axis; they are therefore less affected by the disorder, with all the electron

TABLE 2: Copper Site Coordinates (*x*,*y*,*z*) and Related Crystal Data after Rietveld Refinement[a]

site	*x, y, z*	*D* (Å)	SO	SS	SM	Cu/UC
S_I	0.384, 0.192, 0.260	4.5	0.02(1)	*m*	12	0.24
S_{II}	0.220, 0.220, 0.350[b]	3.0	[b]	*m*	12	[b]
S_{III}	0.0, 0.0, 0.392	0.4	0.08(1)	*6/mm*	2	0.16
S_V	0.0, 0.0, 0.475	0.4	0.07(1)	*6/mm*	2	0.14
S_{VI}	0.230, 0.170, 0.150[b]	5.5	[b]	*1*	24	[b]

[a] *D* = distance from 6-fold axis, SO = site occupancy from Rietveld refinement, SS = site symmetry, SM = multiplicity, Cu/UC = Cu atom per unit cell or supercage, calculated as SO × SM. [b] Occupancy not refinable because of the splitting by symmetry multiplicity, Cu position located with the help of DFT calculations.

density appearing as a single peak, and more easily located in the difference Fourier maps. Sites S_I and S_{II} are quite far (~3.0 to 4.5 Å) from the 6-fold axis (in positions with site symmetry *m* and multiplicity 12) and are therefore much more affected by the disorder (electron density spread over 6 positions by the 6-fold axis) and difficult to locate in the difference Fourier maps, where they appear as very weak peaks. Site S_{VI}, which is even further away (>5 Å) from the 6-fold axis and in a general position with site multiplicity 24, is so affected by the disorder that it cannot be located in the difference Fourier maps. With fixed positions the site occupancy could be refined for sites S_I, S_{III}, and S_V only (see Table 2). The amount of Cu per unit cell (0.54) is smaller than that expected by the unit cell formula (2.27 to balance the charge by the inserted Al atoms) and the remaining amount should be distributed among the 12 equivalent positions of S_{II} and the 24 equivalent positions of S_{VI}. No significant differences in the electron density were observed between the reduced and the oxidized samples.

Copper insertion causes a significant (larger than 5 times the estimated standard deviations) reduction of the *a* lattice parameter and the increase of the *c* parameter, indicating that such a small copper content is able to modify the crystal lattice (Table 1). Conversely there are smaller differences between the reduced and oxidized samples, which are of the order of 2−4 times the estimated standard deviations, thus close to the detection limit. We can therefore conclude that, as expected, the copper oxidation state can only induce very small modifications on the MCM-22 lattice.

The graphic inspection of the structures obtained after Rietveld refinement, in comparison with the copper-free sample, indicates that the most significant effect of the introduction of copper ions (in particular at sites S_{III} and S_V) is the contraction of the 6-MRs of the hexagonal prism, parallel to the (001) plane, with the consequent shortening of the $a = b$ axis (Table 1).

The observed extra-framework peaks in the difference Fourier synthesis were only found within the supercage, independently of the sample pretreatment; no significant electron density was found in the sinusoidal channel at the position of site S_{IV} proposed by Wasowicz et al..[12] This is in agreement with the higher accessibility of the supercage, determined by an NMR study of Xe diffusion.[17] Moreover, three over four sites found by XRPD (S_I, S_{III} and S_V) are related to 6-MRs (Figure 1). The sites determined in this work are found in different parts of the supercage. S_{II}, S_{III}, and S_V are within the narrower part of the cavity, whereas S_I is in the wider part. The Cu ions have different possibilities to access these sites: S_V is embedded in the hexagonal prism (this is the most sterically hindered site), S_{III} faces the hexagonal prism but is already inside the supercage. As a general observation, the residual extra-framework electron density in the difference Fourier syntheses is in accordance with

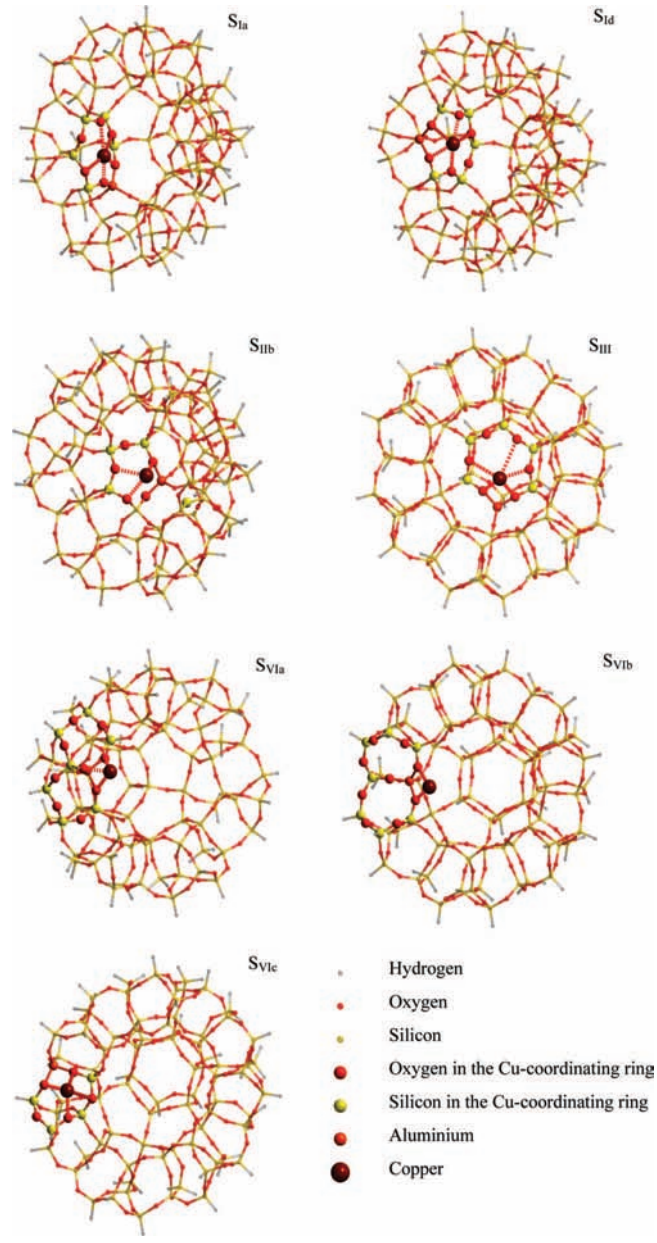

Figure 2. Representative copper sites corresponding to energy minima after full geometry optimization at BLYP/LAV3P* level of calculation (remaining copper-site pictures available as Supporting Information); dotted lines indicate oxygen atoms coordinating Cu ions (corresponding Cu−O distances reported in Table 3) with Cu−O distances smaller than the sum of their vdW radii.

the literature data, since three Cu sites over the four suggested by Wasowicz et al.[12] were found. Nevertheless, as we have seen, reliable values of the position and occupancy of the Cu ion sites could not be obtained by Rietveld refinement of the XRPD data. For instance, Cu site S_{III} must obey the 6-fold rotation symmetry element and the six equivalent Cu−O distances (calculated from the center of mass of the extra-framework electron density to the oxygen atoms) which resulted were equal to 3.2 Å, much larger than the expected values (in the range 1.66−2.35 Å from a CCDC search[44]). Therefore, some ab initio calculations (section 3.2) were carried out to obtain a clearer picture of the geometry and energetic features of the Cu exchange sites inside the supercage of the MCM-22 zeolite.

3.2. Ab Initio Molecular Orbital DFT Calculations. The geometry and energetic features of Cu(I)-ions in all possible exchange sites were investigated by ab initio MO calculations,

TABLE 3: Relative Stability (in kJ/mole) of the Cu Site Models after Geometry Optimization at the Different Levels of Calculations (LAV3P and LAV3P*) and Values Obtained by a Single Point Calculation at the LAV3P* Level, Adopting the LAV3P Geometry (LAV3P*//LAV3P)[a]

Cu site	LAV3P	LAV3P*//LAV3P	LAV3P*	Cu−O distances (Å)	ring	CN[b]
Id	0.0	14.1	0.0	**2.27**, 2.36, 2.42, 2.53, 2.71	6	5
IIb	61.9	47.1	5.0	**2.20**, 2.39, 2.66, 3.16	5	3
III	3.2	0.0	10.9	**2.26**, 2.40, 2.46, 2.60, 2.82	6	5
Ia	16.0	23.8	22.6	**2.16**, 2.53, 2.55, 2.85, 2.88	6	5
Ib	22.0	38.2	30.6	**2.25**, 2.38, 2.39, 2.55	6	4
VIb	41.8	64.0	32.9	**2.18**, **2.19**, 3.14, 3.53	[c]	2
VIc	59.5	58.4	53.4	**2.25**, 2.35, 2.44, 2.63	5	4
IIc	40.7	49.5	55.0	**2.18**, **2.19**, **2.34**, 2.99	5	3
IIa	66.1	49.4	62.9	**2.19**, **2.25**, 2.61, 3.35	5	3
Ic	45.5	55.1	94.5	**2.18**, 2.47, 2.52, 3.12	6	3
VIa	79.0	116.3	113.7	**2.14**, 2.42, 2.45, 3.58	[c]	3

[a] Geometry features (shortest Cu−O distances reported for each site) after LAV3P* geometry optimization: shortest bond distances (<2.35 Å, the largest Cu−O distance found in a CCDC search[44]), compatible with medium/strong Cu−O bonds, are highlighted by bold characters; coordination was established by counting the Cu−O distances shorter than 2.91 Å (sum of the Cu and O atoms vdW radii). [b] CN = coordination number. [c] In between two five-member rings (see text for details).

employing the large cluster models (259 atoms with chemical formula $CuSi_{77}AlO_{132}H_{48}$) depicted in Figure 2, consisting of the same half supercage shown in Figure 1. The Si/Al ratio equal to 15 of the samples employed for XRPD analysis suggests that isolated Al sites are predominant with respect to pairs of [(−Al−O−Si)−] moieties close enough to host Cu(II) cations.[45] Therefore, to assure an isolated Al insertion site, in the employed cluster model only one Al atom was inserted in each cluster, instead of the five needed to have the exact Si/Al ratio of the samples employed in the XPS and XRPD experiments. This model is representative of the reduced outgassed samples employed in the XRPD analysis and consistent with the oxidation state observed by XPS after treatment in UHV (see section 3.4). Given the large size of the model, hybrid QM/MM approaches were tested, but no satisfying cut between the QM and the MM parts was found. Therefore, a full QM approach was chosen for this large cluster, despite its computational cost, because it allowed modelling all Cu sites within the MCM-22 supercage, employing the same model, with a direct indication of the relative stability of the Cu ions inserted in different parts of the supercage. Besides, the large size of the model allowed a full geometry optimization without losing the shape of the supercage. Possible Cu sites bound to oxygen atoms close to the supercage center (near the mirror plane) would be too close to the part where the cluster was truncated from the periodic MCM-22 structure to be correctly described by this model. However, the Cu ion location in this region is unfavoured because the available 10-MRs only allow an unstable two-fold coordination.

Starting from the assumption that stable Cu ion sites require at least a 2 or 3-fold coordination, 30 theoretically possible Cu-site models[46] were generated using the MOLDRAW graphic software.[41] Then 15 out of the 30 models were symmetry equivalent or were unfeasible in the light of chemical and geometry considerations. In fact, optimal Cu sites are the ones stabilized by interactions with the lone pairs of the framework oxygen atoms (those with Cu−O distances in the range 1.90−2.91 Å, i.e., smaller than the sum of their van der Waals (vdW) radii). The remaining 15 models were optimized at the BLYP/LAV3P level. Only 11 out of the 15 models resulted in energy minima and the obtained geometry and energetic parameters of their structures are reported in Table 3, where the obtained Cu sites are compared to the experimental results after Rietveld refinement of the XRPD data and to the literature EPR/ESEM data.[14,16] Different energy minima for the Cu insertion, facing the same ring, are indicated by sequential small letters. Only sites S_I, S_{II}, S_{III}, and S_{VI} are present, because, during geometry optimizations, Cu in site S_V moved to site S_{III}. The final geometries of the more representative Cu sites are depicted in Figure 2 and the remaining ones are available as Supporting Information. Each Cu site has different conformations (depending on the T site where Al is inserted) labeled with letters from a to d (Table 3).

Concerning the level of calculation, the faster LAV3P method was very useful to screen the 30 starting geometries, to single out the energy minima, and to obtain a rough geometry optimizations of the stable Cu sites. Conversely, the relative energies calculated at the LAV3P level do not respect the trend of the higher LAV3P* level calculations, probably because the Cu−O interaction was not well described without the polarization functions, lacking in the calculations at the LAV3P level. Therefore the LAV3P* data only will be used in the following discussion.

The obtained relative energy values indicated that the stability of the Cu ions is more affected by the number of T atoms in the facing ring and by the coordination number than by the particular T site where the Al atom is located. In fact low energy structures are mostly associated to 6-MRs, while Cu in 5-MRs are mostly unstable, especially the S_{VI}-type sites, independently of the Al insertion site: in fact in Table 3 it can be observed that five out of six less stable sites are located close to 5-MRs. It can be concluded that 5-MRs are less well suited to host Cu ions, probably because two out of five oxygen atoms have their electron lone pairs pointing toward the external part of the cavity and are not available for Cu coordination, as can be seen for instance in Figure 2 for site S_{IIb}. Because of these geometry limitations, 5-MRs are mostly associated to copper coordination equal to 2 and 3. Conversely, the 6-MRs (sites S_I- and S_{III}-type) are capable of hosting Cu ions with higher coordination (4 and 5). Only Cu sites with 2- and 3-fold coordination show two short Cu−O contacts, while all Cu sites with 4- and 5-fold coordination show only one short and three to four medium-distance Cu−O contacts (Table 3). In both cases one Cu cation balances one Al anion and the difference is in the degree of delocalization of the negative charge on the oxygen atoms of the 5- or 6-MR. The larger stability of the 4- and 5-fold coordinated sites suggests that in vacuum conditions a larger delocalization is favored. The higher degree of coordination of Cu in 6-MRs was already observed in different zeolites.[21,22] Nevertheless site S_{IIb}, despite its 3-fold coordination, was found

TABLE 4: Indications of Site Stability by DFT Calculations and XRPD and EPR Data

site	DFT	XRPD	EPR
S_I	yes	weak yes	yes
S_{II}	yes	weak yes	yes[a]
S_{III}	yes	yes	yes
S_{IV}	[b]	no	yes
S_V	NEM[c]	yes	yes
S_{VI}	HRE[d]	no	no

[a] Wasowicz et al.[14] suggested a site close to this 5-MR but moved towards the sinusoidal channel. [b] Located into the sinusoidal channel and not in the supercage used for the calculations. [c] NEM = not an energy minimum. [d] HRE = high (>30 kJ/mole) relative energy Cu location site.

TABLE 5: Surface Elemental Analysis by XPS Data Compared to Nominal and Bulk Cu/Al Ratio (Elemental Analysis from Reference 13)

	Cu/Al ratio	
samples	surface	bulk
Ox-CuMCM22	0.5	0.7
Ox-CuMCM22-50	0.1	0.1
H-MCM-22	0	0

rather stable, because of the very short Cu−O distances. Considering Cu sites facing 5 MR's rings, S_{II}-type sites are more stable that S_{VI}-type sites. As can be seen in Table 3, sites of S_I-type can adopt four different arrangements with three different coordinations and sites of S_{VI}-type can adopt three different arrangements with different coordinations and are the most flexible insertion sites. Conversely sites of S_{II}-type with three different arrangements, all with the same coordination, and the only site of S_{III}-type are the least flexible insertion sites. Sites of type S_{VI} have so flexible insertion sites that two of them with 2- and 3-fold coordination move away from the starting position facing a 5-MR and are shared by two adjacent rings (Table 3 and Figure 2).

It is worth noting that the Cu−O bond distances obtained after the geometry optimization (Table 3) are in agreement with those reported in the literature. In fact, after a search of Cu−O containing structures in the CCDC database,[44] 139 Cu−O distances were found ranging from 1.66 to 2.35 Å, with an average Cu−O distance of 1.95(7). Concerning the coordination number and geometry, the Cu sites can be divided into four categories: (i) pentacoordinated sites in 6-MRs; (ii) tetracoordinated sites, with one Cu−O short contact (<2.35Å, in the range of Cu−O bond distances found in a CCDC search) and three medium-distance contacts (between 2.35 and 2.92 Å); (iii) three-coordinated sites with one or two Cu−O short contacts; (iv) bi-dentate Cu site (S_{VIb}) with one or two short Cu−O distances but with the other Cu−O distances far larger than the sum of the vdW radii. It is worth noting that sites S_{VIa} and S_{VIb} are the most accessible ones, pointing toward the central part of the supercage.

3.3. Comparison between EPR, XRPD, IR, and DFT Computational Data. The indications of the XRPD data and the QM calculations, together with the EPR data from the literature,[14,16] (summarized in Table 4) suggested that there are five possible insertion sites for the copper location in the supercage of MCM-22 (Figure 1). QM calculations allowed finding 11 minimum energy conformations (Table 3, Figure 2) in these 5 insertion sites. However, among the five sites, three (S_I, S_{II}, and S_{III}) are suggested by all experimental and theoretical techniques and can be considered preferentially occupied in copper-exchanged MCM-22 under vacuum conditions. In fact at low Cu loading (the under-exchanged Ox-CuMCM22-50 sample in Table 1) S_{III} and S_V are the only occupied sites. S_V, which is found by XRPD and EPR, is not an energy minimum after quantum-chemical calculations as already observed in CHA zeolite.[21] However, it is located inside the hexagonal prism, close to S_{III} and not accessible to molecule adsorption and can be therefore considered of secondary importance. Site S_{II} is suggested by EPR and XRPD (but located into the sinusoidal channel by EPR) while S_{VI} is inferred by theoretical calculation only. Both sites are simulated, with smaller Cu coordinations and in general smaller energy stability. Indeed, water molecules or adsorbed gases might affect the relative stability of these sites, favouring the less coordinated bi- and tetradentated sites, located in the more accessible interlamellar space, but this does not apply to the outgassed Cu-MCM22 samples, employed in the XRPD and XPS experiments, the results of which are compared to the theoretical calculations. The proved presence of three types of possible Cu sites with different coordination geometries is therefore able to give a structural explanation of the IR data reported by some of us,[12] which suggested that two copper families with different bonding energy toward NO are present in Cu-MCM-22. The broadening of the IR bands,[12] even at liquid nitrogen temperature, can be explained by the fact that more Cu sites are populated in each family (Cu in 5- or 6-MRs) of sites.

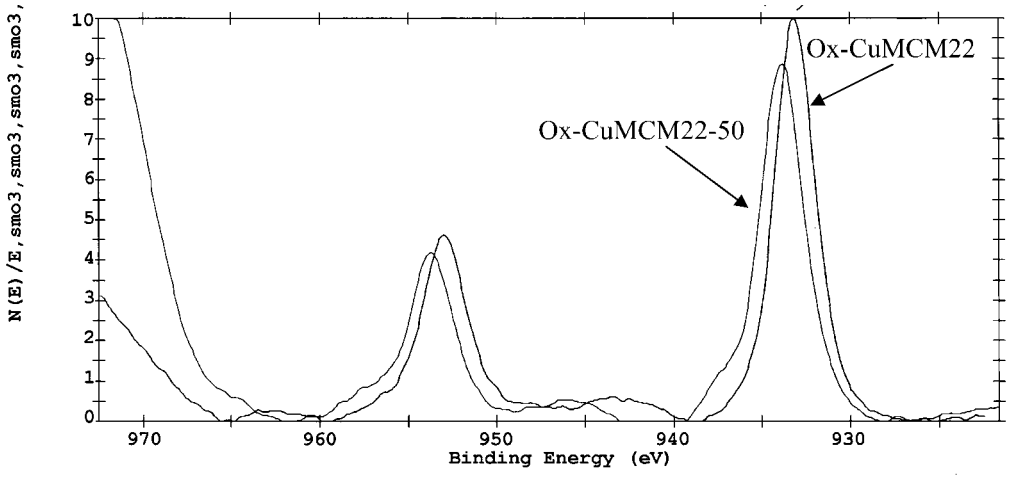

Figure 3. Cu 2p 3/2 and 1/2: peaks for Ox-CuMCM22-50 and Ox-CuMCM22 in the XPS analysis.

The combined computational and X-ray diffraction structural analysis allowed a definition of the local structure of copper ions and their distribution within the MCM-22 zeolite cages in the bulk of the MCM-22 crystallites together with their energetic features. The absence of peaks due to dense CuO phases in the examined samples assures us that copper is not significantly aggregated and is distributed within the MCM-22 cavities. Therefore in the reduced sample, isolated Cu−Al couples are formed, as described by the theoretical calculations. In the oxidized sample, the situation is complicated because no simple explanation can be found to attain the charge balance. Concerning the copper excess, four situations can be envisaged: (i) insertion of Cu(II) close to one Al atom and close to negatively-charged defects; (ii) formation of cationic dimers $(Cu-O-Cu)^{+2}$ as a function of the ion exchange procedure; [47,48] (iii) decomposition of the dimers in ii according to the reaction: $(Cu-O-Cu)^{+2} \rightarrow 2\ Cu^{+} + {}^{1}/_{2}O_2$;[49] (iv) formation of cationic copper aggregates in MCM-22 channels, assuming an oligomeric $Cu-(O-Cu)_n$ structure of small size not detectable by XRPD as a separated CuO phase. To clarify these points, XPS analyses were performed to estimate the Cu concentration and chemical state on the surface of the MCM-22 crystals in the oxidized under-(Ox-CuMCM22-50) and over-(Ox-CuMCM22) exchanged samples.

3.4. X-ray Photoelectron Spectroscopy. XPS data allowed an estimation of the Cu/Al ratio on the crystallite surface and the results are reported in Table 5. From these data we can conclude that the copper excess is not concentrated as nanoclusters on the surface, where concentrations smaller than those observed in the bulk are detected.

High-resolution analysis of the Cu 2p peaks in the two cases shows relatively narrow components (fwhm = 2.8 eV), occurring at 933.2 eV (150% Cu) and at 933.9 eV (50% Cu) The presence of only two peaks (Cu2p 3/2 and Cu2p 1/2) in the spectrum (Figure 3) suggests that the electronic configuration of copper is d^{10} in both cases, that is, Cu(I). Besides Cu(II), with electronic configuration d^9 can be excluded by the absence of the typical two additional "shake-up" satellites.[50] Metallic Cu can be excluded because its peak would be around 932.6 eV. Separation of dense copper phases is also excluded by the XRPD data, indicating that only the MCM-22 phase is present. From these data we can conclude that surface Cu ions have a first coordination shell similar to CuO, but with the electronic structure being more similar to Cu(I),[50] suggesting that UHV is able to promote the reduction of Cu(II) ions.

4. Conclusions

The full profile Rietveld refinement of the XRPD patterns collected on Cu-MCM22 samples with ratio Cu/Al = 0.71, together with the QM calculations, allowed us to locate 5 extra-framework Cu sites with 11 possible minimum energy conformations. Three Cu sites (S_I, S_{III}, and S_V) facing 6-MRs and two (S_{II} and S_{VI}) facing 5-MRs were located inside the MCM-22 supercage. The qualitative information on the Cu sites by EPR and IR data were interpreted quantitatively and, for the first time, the geometry and energetic data for all the Cu insertion sites in the supecage were obtained, thanks to the exhaustive DFT study carried out. No Cu ions were found within the sinusoidal channels by XRPD. This is in agreement with ^{129}Xe NMR experiments reported in the literature,[17] suggesting that the sinusoidal channels are less accessible. Ab initio DFT calculations gave information on the geometry and energetic features of the copper insertion sites, which confirmed and complemented the indications suggested by XRPD and EPR data. Cu(I) sites facing 6-MRs were particularly stable. In general 5- or 4-fold coordination sites are located in 6-MRs while 2- or 3-fold coordination sites are located in 5-MRs, and this fact could explain the larger stability of Cu sites inserted in six-membered rings. The most stable sites in these isolated cluster calculations are the penta- and tetracoordinated S_I- and S_{III}-type. Considering XRPD and theoretical data, three sites (S_I, S_{II}, and S_{III}-type) are preferentially occupied in copper-exchanged MCM-22. XPS measurements excluded the formation of Cu nanoaggregates close to the surface and indicated that in UHV conditions, Cu is present at the MCM-22 surface in a d^{10} electronic configuration, which can be sustained by low oxygen coordination.

The combined computational, XRD, and XPS investigations allowed us to define the local structure of copper ions and their distribution within the MCM-22 zeolite cages and to obtain a comparison between bulk and surface of the MCM-22 crystallites. The obtained stable model clusters can be used for further theoretical investigations of the catalytic properties of Cu sites interacting with gases and/or water in the supercages of MCM22, as well as in related solids such as the delaminated ITQ-2 or swollen ITQ-36.

Acknowledgment. This work was funded by the Italian MURST in the frame of the "*Progetti di Rilevante Interesse Nazionale*" (PRIN, Cofin2002") and the Brazilian FAPESP ("*Fundação de Amparo à Pesquisa no Estado de São Paulo*"). The authors are deeply indebted to Prof. L. Marchese (Università del Piemonte Orientale) for useful discussions, to Dr. W. van Beek (Swiss-Norwegian beamline at the ESRF) for the precious support during the XRPD data collection, and to Prof. G. Artioli (Università di Milano) for useful suggestions on the XRPD data analysis. ESRF is acknowledged for beam time (experiments CH-1423 and CH-1535).

Supporting Information Available: 3-D pictures of the Cu-sites models not depicted in Figure 2. Atomic coordinates of the Cu-containing MCM-22 crystal structure. Atomic coordinates of the 11 molecular clusters after DFT geometry optimization (Moldraw format, see ref 41). This material is available free of charge via the Internet at http://pubs.acs.org.

References and Notes

(1) Meier, W. M.; Olson, D. H.; Baerlocher, C. H. *Atlas of Zeolite Structure Types*; Elsevier: London, 1996.
(2) Rubin, M. K.; Chu, P. US Patent 4 954 325 (1990).
(3) Corma, A.; Fornés, V.; Pergher, S. B.; Maesen, Th. L. M.; Burglass, J. G. *Nature* **1998**, *378*, 353.
(4) Lawton, S. L.; Leonowicz, M. E.; Partridge, R. D.; Chu, P.; Rubin, M. K. *Microporous Mesoporous Mater.* **1998**, *23*, 109.
(5) Leonowicz, M. F.; Lawton, J. A.; Lawton, S. L.; Rubin, M. K. *Science* **1994**, *264*, 1910.
(6) Nicolopoulos, S.; González-Calbet; J, M.; Vallet-Regi, M.; Corma, A.; Corell, C.; Guil, J.M.; PéreParient, J. *J. Am. Chem. Soc.* **1995**, *17*, 8947.
(7) Corma, A.; Corell, C.; Martinez, A.; Pérez-Pariente, J. *Stud. Surf. Sci. Catal.* **1994**, *84A*, 1671.
(8) Li, Y.; Armor., J. N. *Appl. Catal. B* **1992**, *1*, L21.
(9) Palella, B. I.; Pirone, R.; Russo, G.; Albuquerque, A.; Pastore, H. O.; Cadoni, M.; Frache, A.; Marchese, L. *Catal. Commun.* **2004**, *5*, 191.
(10) Guisnet, M. ; Ribeiro, F. R. *Zeólitos: Um Nanomundo a Serviço da Catálise*; Fundação Calouste Gulbenkian: Lisbon, Spain, 2004; p 36.
(11) Absil, R. P. L.; Bowes, E.; Green, G. J.; Marler, D. O.; Shihabi, D. S.; Socha, R. F. US Patent 5 085 762, 1992.
(12) Frache, A.; Cadoni, M.; Bisio, C.; Marchese, L.; Mascarenhas, A. J. S.; Pastore, H. O. *Langmuir* **2002**, *18*, 6875.
(13) Mascarenhas, A. J. S.; Pastore, H. O.; Andrade, H. M. C.; Frache, A.; Cadoni, M.; Marchese, L. *Stud. Surf. Sci. Catal.* **2002**, *142A*, 343.
(14) Wasowicz, T.; Prakash, A. M.; Kevan, L. *Microporous Mater.* **1997**, *12*, 107.

(15) Prakash, A.M.; Wasowicz, T.; Kevan, L. *J. Phys. Chem. B* **1997**, *101*, 1985.

(16) Umamaheswari, V.; Hartmann, M.; Püppl, A. *J. Phys. Chem. B* **2005**, *109*, 1537.

(17) Chen, F.; Deng, F.; Cheng, M.; Yue, Y.; Ye, C.; Bao, X. *J. Phys. Chem. B* **2001**, *105*, 9426.

(18) Sastre, G.; Fornes, V.; Corma, A. *J. Phys. Chem. B* **2000**, *104*, 4349.

(19) Wang, Y.; Zhou, D.; Yang, G.; Miao, S.; Liu, X. Bao. *J. Phys. Chem. A* **2004**, *108*, 6730.

(20) Zheng, A.; Chen, L.; Yang, J.; Zhang, M.; Su, Y.; Yue, Y.; Ye, C.; Deng, F. *J. Phys. Chem. B* **2005**, *109*, 24273.

(21) Solans-Monfort, X.; Branchadell, V.; Sodupe, M.; Zicovich-Wilson, C.M.; Gribov, E.; Spoto, G.; Busco, C.; Ugliengo, P. *J. Chem. Phys. B* **2004**, *108*, 8278.

(22) Nachtigall, P.; Nachtigallova, D.; Sauer, J. *J. Phys. Chem. B* **2000**, *104*, 1738.

(23) Davidova, M.; Nachtigallova, D.; Nachtigall, P.; Sauer, J. *J. Phys. Chem. B* **2004**, *108*, 13674.

(24) Bludský, O.; Sihlan, M.; Nachtigall, P.; Bucko, T.; Benco, L.; Hafner, J. *J. Phys. Chem. B* **2005**, *109*, 9631.

(25) Lamberti, C.; Bordiga, S.; Salvalaggio, M.; Spoto, G.; Zecchina, A.; Geobaldo, F.; Vlaic, G.; Bellatreccia, M. *J. Phys. Chem. B* **1997**, *101*, 344.

(26) Da Costa, P.; Moden, B.; Meitzner, G. D.; Lee, D. K.; Iglesia, E. *Phys. Chem. Chem. Phys.* **2002**, *18*, 4590.

(27) Turnes Palomino, G.; Bordiga, S.; Zecchina, A.; Marra, G. L.; Lamberti, C. *J. Phys. Chem. B* **2000**, *104*, 8641.

(28) Fowkes, A. J.; Ibberson, R. M.; Rosseinsky, M. J. *Chem. Mater.* **2002**, *14*, 590.

(29) Haniffa, R. M.; Seff, K. *Microporous Mesoporous Mater.* **1998**, *25*, 137.

(30) Jardiller, N.; Ayala Villagomez, E.; Delahay, G.; Coq, B.; Berthomieu, D. *J. Phys. Chem. B* **2006**, *110*, 16413.

(31) Iwamoto, M.; Yahiro, H.; Torikai, Y.; Yoshoka, T.; Mizuno, N. *Chem. Lett.* **1990**, 1967.

(32) Milanesio, M.; Croce, G.; Frache, A.; Mascarenhas, A. J. S.; Oliveira, E. C. *Stud. Surf. Sci. Catal.* **2005**, *155*, 415.

(33) Proposal CH-1423. Experiment carried out at the BM1B at the SNBL (ESRF; web site http://www.esrf.fr); information on the beamline setup can be found on the web site http://www.snbl.eu.

(34) Larson, A. C.; Von Dreele, R. B. *General Structure Analysis System (GSAS)*; Los Alamos National Laboratory, Report LAUR; Los Alamos National Laboratory: Los Alamos, NM, 2000; Vol. 8, pp 6−748 (http://www.ccp14.ac.uk/solution/gsas/index.html).

(35) *Jaguar 5.5*, version 5.5; Schrödinger Inc.: Portland, OR, 2003.

(36) Becke, A. D. *J. Chem. Phys.* **1988**, *38*, 3098.

(37) Lee, C.; Yang, W.; Parr, R. G. *Phys. Rev. B* **1988**, *37*, 785.

(38) (a) Hay, P. J.; Wadt, W. R. *J. Chem. Phys.* **1985**, *82*, 270. (b) Wadt, W. R.; Hay, P. J. *J. Chem. Phys.* **1985**, *82*, 284.

(39) Hehre, W. J.; Radom, L.; Schleyer, P. v. R.; Pople J. A. *Ab Initio Molecular Orbital Theory;* Wiley: New York, 1986.

(40) Yuan, S. P.; Wang, J. G.; Li, Y. W.; Jiao, H. *J. Phys. Chem. A* **2002**, *106*, 8167.

(41) (a) Ugliengo, P.; Viterbo, D.; Chiari, G. *Z. Krist.* **1993**, *207*, 9. (b) Moldraw: A Program to Display and Manipulate Molecular and Crystalline Structures; http:/www.moldraw.unito.it. (accessed April 25, 2008).

(42) *MAESTRO*, version 7.0.105; Schrödinger, Inc: Portland, OR, 1999−2005.

(43) (a) Moulder, J. F.; Stickle, W. F.; Sobol, P. E.; Bomben, K. D. *Handbook for XPS*; Physical Electronics: Eden Prairie, MN, 1992. (b) NIST Binding Energies Database; http://srdata.nist.gov/XPS. (accessed April 25, 2008).

(44) Allen, F. H. *Acta Cryst.* **2002**, *B58*, 380.

(45) Teraishi, K.; Ishida, M.; Irisawa, J.; Kume, M.; Takahashi, Y.; Nakano, T.; Nakamura, H.; Miyamoto, A. *J. Phys. Chem. B* **1997**, *101*, 8079.

(46) The number of theoretically possible sites was calculated starting from the 7 symmetry-independent Al substitution sites, available in the supercage; then we assumed that each Al atom is bonded to 4 oxygen atoms, each carrying 2 lone pairs apt to bind copper: therefore the number of possible copper substitution sites is $7 \times 4 \times 2 = 56$; however, some of the O atoms are shared between framework T sites and therefore the true theoretical number of possible Cu sites reduces to 30.

(47) Mascarenhas, A. J. S.; Andrade, H. M. *React. Kinet. Catal. Lett.* **1998**, *64*, 215.

(48) Centi, G.; Perathoner, S. *Appl. Catal. A* **1995**, *132*, 179.

(49) Iwamoto, M.; Maruyama, K.; Yamazoe, N.; Seyama, T. *J. Phys. Chem.* **1997**, *81*, 622.

(50) (a) Bolis, V.; Maggiorini, S.; Meda, L.; D'Acapito, F.; Turnes Palomino, G.; Bordiga, S.; Lamberti, C. *J. Chem. Phys.* **2000**, *113*, 9248. (b) Meda, L.; Ranghino, G.; Moretti, G.; Cerofolini, G. F. *Surf. Interf. Anal.* **2002**, *33*, 516.

JP803619R